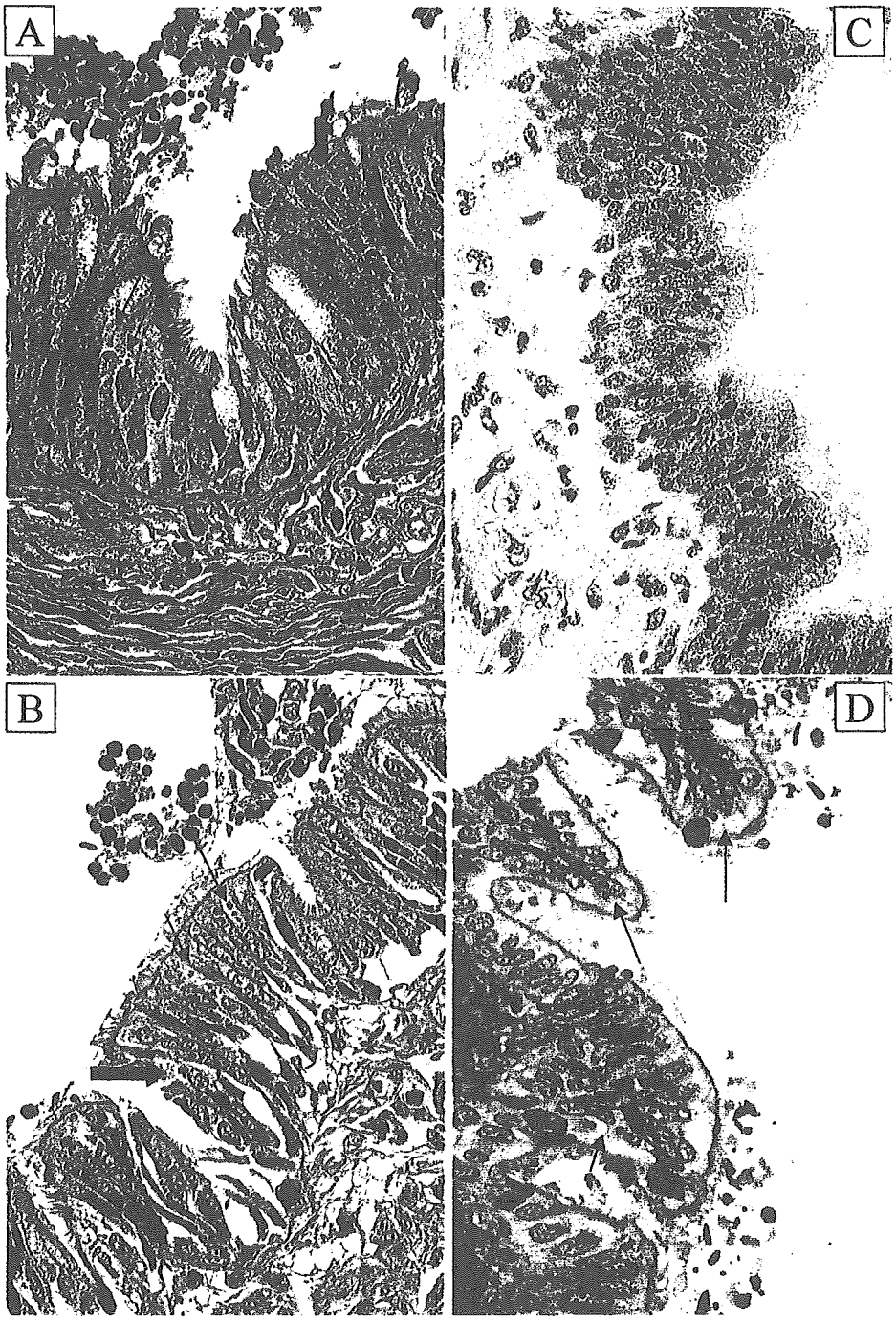

Figure 1. Cytoplasmic inclusion bodies are visible by light microscopy in acute Kawasaki disease (KD) ciliated bronchial epithelium. *A* and *B*, hematoxylin-eosin–stained sections from patients 4 and 6 showing amphophilic spheroidal cytoplasmic inclusion bodies *(thin arrows)* and irregular, golden yellow, granular, supranuclear pigment resembling classic lipofuscin *(thick arrows)*. *C*, Immunohistochemistry-stained section from patient 3 demonstrating brown, spheroidal, cytoplasmic inclusion bodies identified with synthetic KD antibody J. *D*, Methylene blue/azure II/basic fuchsin trichrome–stained section from patient 2 showing dark blue cytoplasmic inclusion bodies; goblet cells stained red. Original magnifications, ×640 for all panels.

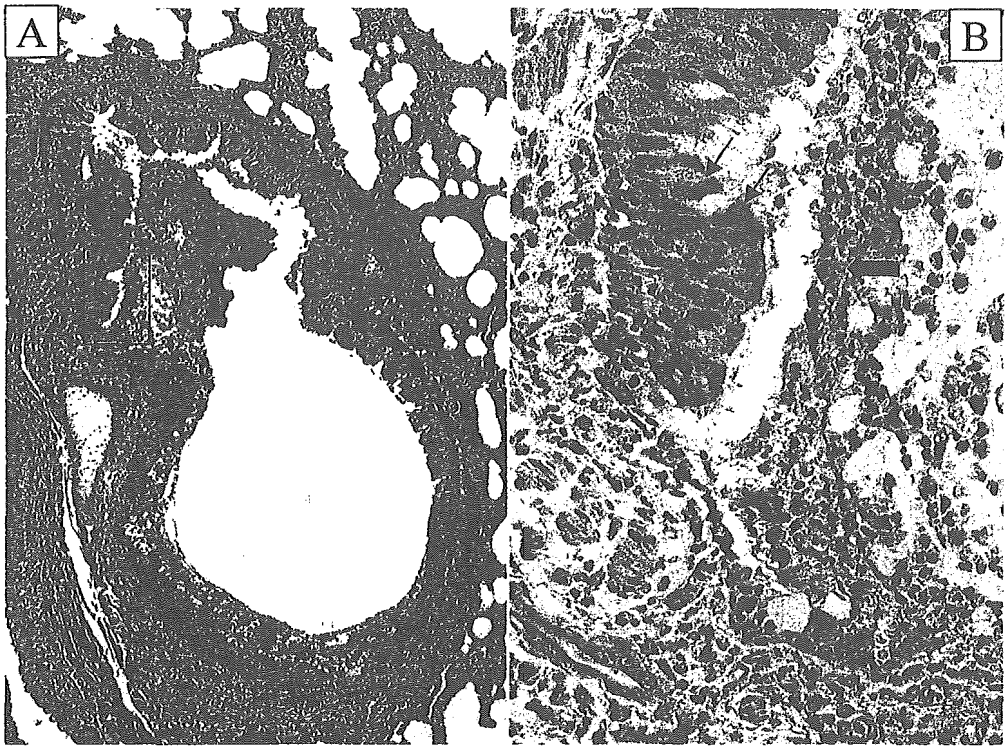

Figure 2. Detection of antigen in inflamed, partially necrotic bronchus from patient 4. *A,* Hematoxylin-eosin stain of bronchus. Most of the right side of the bronchus shows inflammation with intact epithelium; the bottom and most of the left side of the bronchus is devoid of epithelial cells, which have been replaced by an inflammatory exudate that spills over into the lumen. *B,* Immunohistochemistry-stained section, with synthetic Kawasaki disease antibody J, corresponding to the boxed area indicated in panel A. It demonstrates brown antigen in the remaining bronchial epithelial cells *(thin arrows)* and in the cytoplasm of a macrophage located in the adjacent inflammatory exudate *(thick arrow).* Original magnifications, ×40 for panel A and ×640 for panel B.

II/basic fuchsin trichrome stain (figure 1), indicating very concentrated protein and/or nucleic acid accumulation.

TEM. For patients 1–4, homogeneous, relatively regular, electron-dense inclusion bodies (up to 1.4 microns in diameter) were observed in the perinuclear region of the ciliated bronchial epithelial cells. Inclusion bodies were not present in nonciliated cells. These structures resembled the intracytoplasmic aggregates of viral proteins/nucleic acids, such as nucleocapsid aggregates, that are observed during infection with many RNA viruses (figures 3 and 4) [9–13]. Because membranes do not survive postmortem degeneration and the paraffin-embedding process, it was not possible to determine whether the inclusion bodies were membrane bound. Furthermore, these harsh conditions would undoubtedly obscure any ultrastructural features of virus-related structures that might be present in the inclusion bodies, for example, nucleocapsids and virions. Nothing resembling intranuclear inclusion bodies or viral components was identified in the nucleus. A section of the IHC-stained block face from patient 1 was compared with the TEM image from that area; excellent correlation was observed between the inclusion bodies identified by IHC and the electron-dense inclusion bodies observed by TEM (figure 3). In patients 1, 3, and 4, in addition to inclusion bodies, many smaller, pleomorphic, electron-dense bodies were also observed. These structures were mostly homogeneous, unlike typical lipofuscin. No structures resembling bacterial, fungal, or parasitic elements were observed by TEM in the inclusion bodies, the epithelial cells, or the ciliated border external to the cells from patients 1–4.

DISCUSSION

In the present study, we report that LM and TEM demonstrate that synthetic KD antibodies A and J detect intracytoplasmic inclusion bodies in acute KD ciliated bronchial epithelial cells. The inclusion bodies are consistent with aggregates of viral proteins that are likely to be associated with nucleic acid. These results provide new insights into the etiology and pathogenesis of acute KD, and they suggest new directions for identification of the etiologic agent.

Although the coronary arteries are the most clinically significant site of inflammation in patients with acute KD, pathological studies indicate a high incidence of inflammatory lesions in many organs and tissues, including the lungs [14]. The epidemiologic

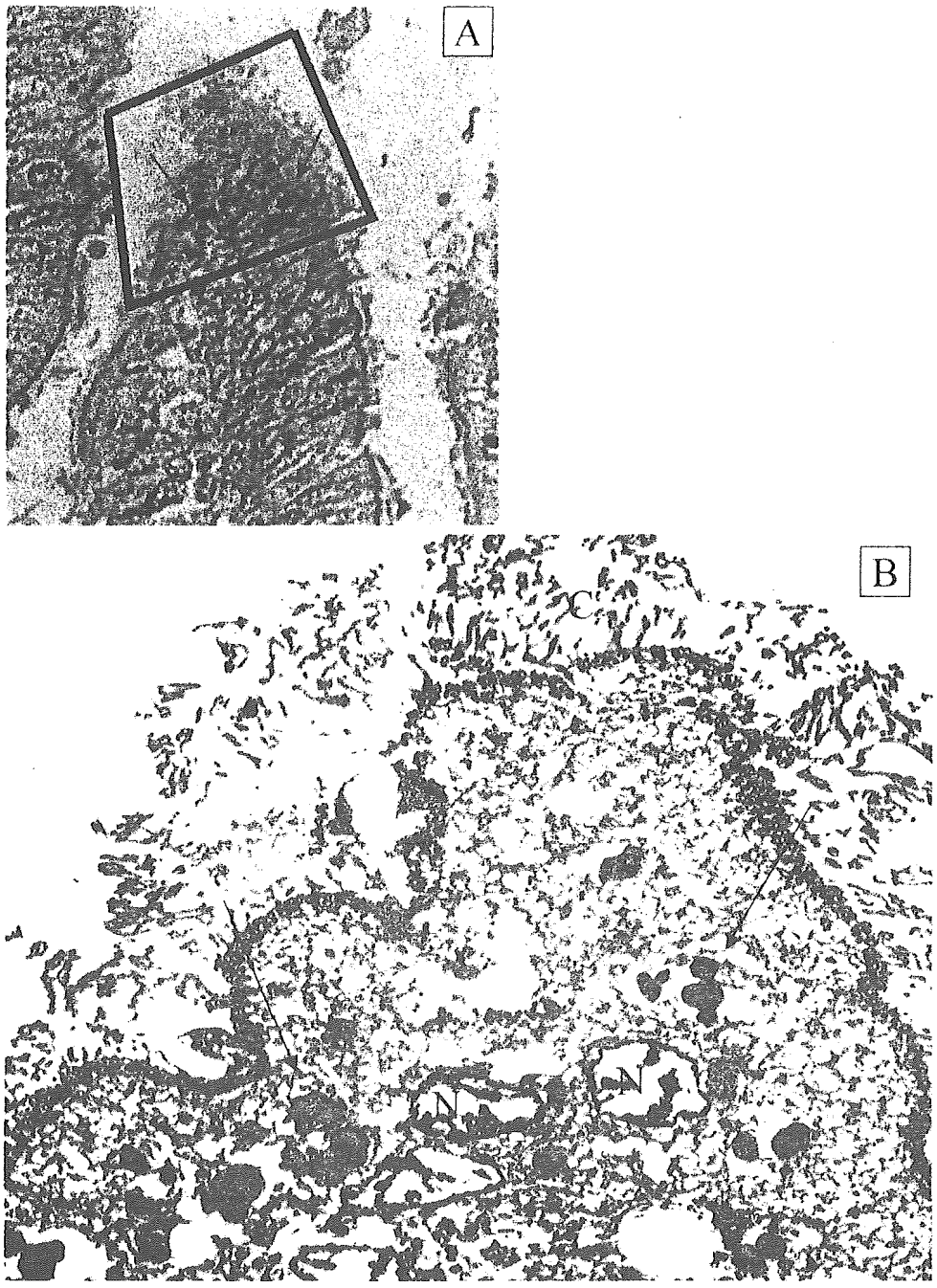

Figure 3. Correlation of cytoplasmic inclusion bodies as demonstrated by immunohistochemistry (IHC) and transmission electron microscopy (TEM). *A,* IHC block face from patient 1 demonstrating IHC-positive inclusion bodies *(arrows). B,* Homogeneous perinuclear inclusion bodies *(arrows)* demonstrated by TEM correspond to inclusion bodies demonstrated by IHC. The thickness of the TEM section is 0.08 microns, and the thickness of the IHC section is 5 microns; therefore, not all structures present in the IHC section can be observed in the TEM section. Original magnifications, ×500 for panel A and ×2000 for panel B. C, cilia; N, nucleus.

profile of KD supports a ubiquitous etiologic agent, and most ubiquitous infectious agents enter the body through either the respiratory or the gastrointestinal tract. The infiltration of IgA plasma cells into the upper respiratory tract in patients with acute KD occurs in a pattern similar to that generally observed during respiratory viral infections [4]. The predominance of CD8 T lymphocytes in the inflammatory cell infiltrate during acute KD [5] implicates an intracellular pathogen as the etiologic agent. Our discovery that synthetic antibodies A and J bind to intracytoplasmic inclusion bodies in acute KD ciliated bronchial epithelium leads to speculation that the antibodies bind to antigens derived from the etiologic agent of KD and that the site of

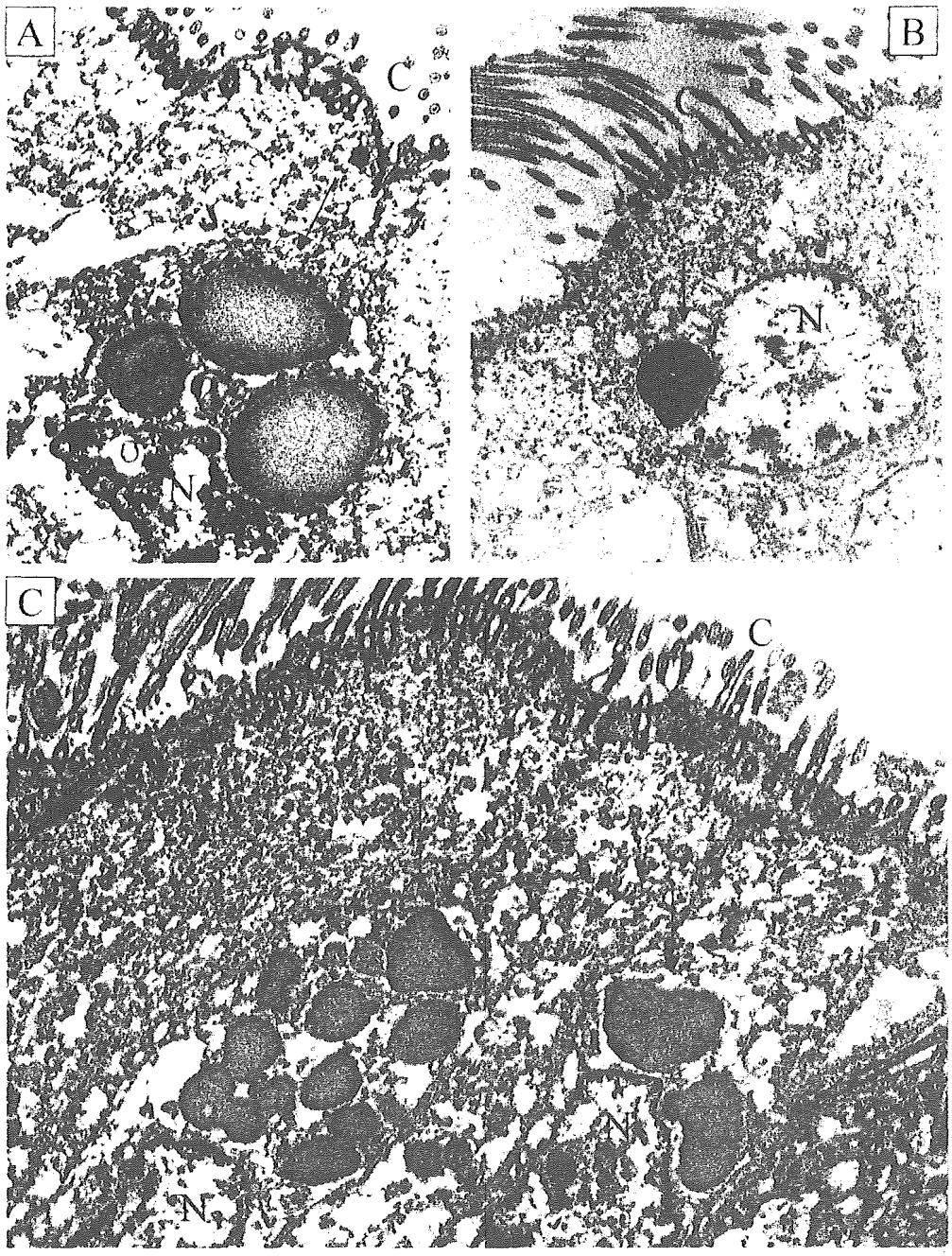

Figure 4. Homogeneous cytoplasmic perinuclear inclusion bodies observed by transmission electron microscopy in patients 2–4. *A,* Three regular, homogeneous perinuclear inclusion bodies *(arrow)* are observed in a ciliated bronchial epithelial cell from patient 3. *B,* A single homogeneous spheroidal inclusion body *(arrow)* is observed indenting the nucleus of a ciliated bronchial epithelial cell from patient 2. *C,* Multiple homogeneous bodies *(arrows)* are observed in ciliated bronchial epithelial cells from patient 4. Original magnifications, ×17,000 for panel A and ×14,000 for panels B and C. C, cilia; N, nucleus.

primary infection for acute KD may be the medium-sized bronchi of the lungs. Although limited TEM studies have been performed on lymph nodes, kidneys, conjunctivae, and peripheral blood from patients with acute KD [15–18], the lungs have not been examined. However, if the lungs are the site of primary infection for acute KD, examination of this tissue could be particularly important to understanding the disease's pathogenesis. Therefore, we studied ciliated bronchial epithelial cells from patients with acute KD by LM and TEM.

The normal ciliated bronchial epithelial cell is highly polarized, with an electron-dense nucleus and mostly electron-lucent cytoplasm. The rough endoplasmic reticulum and the Golgi complex are mostly apical and are adjacent to the nucleus. Small numbers of lysosomes can be present in the apical cy-

face, to provide energy for the cilia. Inclusion bodies are observed in the apical cytoplasm of mammalian ciliated bronchial epithelial cells infected with RNA viruses, particularly those belonging to the *Paramyxoviridae* family [8]; these inclusion bodies represent aggregates of nucleocapsids.

Rapid, neutral-buffered glutaraldehyde fixation of fresh tissues is optimal for TEM, with rapid, neutral-buffered formalin fixation being second best. The tissue available to us from patients with acute KD was formalin fixed at autopsy and then embedded in paraffin and was, thus, exceedingly suboptimal for ultrastructural study. When TEM is performed on such material, cellular details such as membranes, cytoplasmic organelles, and infectious agents (especially viruses) are poorly preserved, at best. Although inclusion bodies consistent with aggregates of viral protein were observed in acute KD ciliated bronchial epithelial cells, viral particles or nucleocapsids were not identified, which, given the state of the tissue, does not rule out their presence.

Immune electron microscopy with gold beads is the optimal technique for confirming that the inclusion bodies observed by IHC are the same as the inclusion bodies observed by TEM; however, this technique is best suited to fresh tissues, which are virtually unavailable. Therefore, we aligned TEM images with the IHC-stained tissue block face and demonstrated that the inclusion bodies identified by the 2 techniques represented the same structures.

Inclusion bodies were predominantly observed in ciliated bronchial epithelial cells of medium-sized, compared with larger or smaller, bronchi. Recent evidence indicates that many respiratory viruses preferentially infect ciliated bronchial epithelial cells, potentially because they use certain sialic acid residues as receptors that are expressed only by ciliated epithelial cells [19, 20].

The detection of golden yellow, lipofuscin-like pigment in ciliated bronchial epithelium from some patients with acute KD was, at first, puzzling. Classic lipofuscin is an age-related pigment—it is especially seen in adult liver, brain, and heart—and consists of oxidatively modified cross-linked proteins originating from autophagocytized, indigestible cytoplasmic components [21]. Although accumulations of lipofuscin can be observed in the neurons of children with neuronal ceroid lipofuscinosis, we were unable to find a precedent for accumulations of lipofuscin-like material in tissues from otherwise healthy infants or even infants with other respiratory infections (such as RSV infection), particularly in bronchial epithelium. The lower quantity of pigment detected by Fontana stain, compared with that observed as golden yellow granular pigment detected by HE stain, and the relatively small pleomorphic brown bodies observed in the IHC preparations suggest that the pigment observed in HE-stained sections is not classic, age-related lipofuscin but rather may be pigment formed during a process of lysosomal degradation of large quantities of protein in inclusion bodies. The major cytoplasmic pathway used by eukaryotic cells to selectively degrade excess proteins is ubiquitin-dependent proteolysis in the proteasome. Proteins not degraded by proteasomes can be autophagocytized, further oxidized within lysosomes, and, therefore, partly converted into lipofuscin. It is possible that excessive viral protein produced in the bronchial epithelial cells cannot be handled by the proteasome and that, as a result, lysosomal activity is increased. Alternatively, several viruses—such as adenovirus [22], herpesviruses [23], and, potentially, severe acute respiratory syndrome coronavirus (CoV) [24]—may produce proteins that interfere with proteasome function to their advantage. Proteasome inhibition has been shown to enhance lipofuscin formation [25]. Thus, the etiologic agent of KD may interfere with proteasome function, resulting in increased lysosomal degradation of its proteins and resultant lipofuscin-like deposits containing undigested viral material.

Because synthetic antibodies A and J both bind to inclusion bodies in ciliated bronchial epithelial cells in patients with acute KD, and because both show binding to tissues from the same patients with acute KD, it is likely that these antibodies bind to the same or different epitopes of a single antigen. The detection of the inclusion bodies by synthetic monoclonal KD antibodies implies that KD results from infection with a single respiratory viral agent or a group of very closely related viral agents, as we suggested in our previous study [7]. A recent study reported detection of human CoV (HCoV) NL63 in respiratory samples from patients with acute KD by reverse-transcriptase polymerase chain reaction [26], but we, in collaboration with an international multicenter group of collaborators [27], and at least 2 other independent groups of investigators [28, 29] have subsequently tested respiratory samples from children with acute KD from diverse geographic locations and reported that acute KD is not associated with HCoV-NL63. Therefore, we believe that it is unlikely that the inclusion bodies we observed are the result of infection with HCoV-NL63.

We suspect that KD likely results from infection with an as-yet unidentified viral agent. Identification of the antigen detected by use of synthetic KD antibodies A and J in acute KD tissues has been considerably hampered by the lack of fresh tissue samples available for analysis. Deaths from acute KD are rare but continue to occur worldwide. It will be critical to obtain glutaraldehyde-fixed tissue samples from future fatalities so that more-optimal ultrastructural experiments can be performed. Identification of the structure of any viral particles observed could be critical in narrowing the search for a viral etiologic agent. In the meantime, we are using various molecular methods to analyze formalin-fixed tissues in an effort to determine the nature of the viral proteins and/or nucleic acids present in the inclusion bodies.

Acknowledgment

We acknowledge the excellent histological work of Leslie Kiefer.

References

1. Rowley AH. Kawasaki syndrome. In: Gershon AA, Hotez PJ, Katz SL, eds. Krugman's infectious diseases of children. 11th edition. Philadelphia: Mosby, **2004**:323–35.
2. Newburger JW, Takahashi M, Gerber MA, et al. Diagnosis, treatment, and long-term management of Kawasaki disease. Circulation **2004**; 110:2747–71.
3. Rowley AH, Eckerley CA, Jack HM, Shulman ST, Baker SC. IgA plasma cells in vascular tissue of patients with Kawasaki syndrome. J Immunol **1997**; 159:5946–55.
4. Rowley AH, Shulman ST, Mask CA, et al. IgA plasma cell infiltration of proximal respiratory tract, pancreas, kidney, and coronary artery in acute Kawasaki disease. J Infect Dis **2000**; 182:1183–91.
5. Brown TJ, Crawford SE, Cornwall M, Garcia F, Shulman ST, Rowley AH. CD8 T cells and macrophages infiltrate coronary artery aneurysms in acute Kawasaki disease. J Infect Dis **2001**; 184:940–3.
6. Rowley AH, Shulman ST, Spike BT, Mask CA, Baker SC. Oligoclonal IgA response in the vascular wall in acute Kawasaki disease. J Immunol **2001**; 166:1334–43.
7. Rowley AH, Baker SC, Shulman ST, et al. Detection of antigen in bronchial epithelium and macrophages in acute Kawasaki disease by use of synthetic antibody. J Infect Dis **2004**; 190:856–65.
8. *Paramyxoviridae.* In: Murphy FA, Gibbs EPJ, Horzinek MC, Studdert MJ, eds. Veterinary virology. 3rd edition. San Diego: Academic Press, **1999**:411–28.
9. Bryson DG, McNulty MS, McCracken RM, Cush PF. Ultrastructural features of experimental parainfluenza type 3 virus pneumonia in calves. J Comp Path **1983**; 93:397–414.
10. Goldsmith CS, Tatti KM, Ksiazek TG, et al. Ultrastructural characterization of SARS coronavirus. Emerg Infect Dis **2004**; 10:320–6.
11. Gilka F, Spencer J. Viral matrix inclusion bodies in myocardium of lymphoid leukosis virus-infected chickens. Am J Vet Res **1985**; 46: 1953–60.
12. Hyatt AD, Selleck PW. Ultrastructure of equine morbillivirus. Virus Res **1996**; 43:1–15.
13. Wong KT, Shieh WJ, Kumar S, et al. Nipah virus infection: pathology and pathogenesis of an emerging paramyxoviral zoonosis. Nipah Virus Pathology Working Group. Am J Pathol **2002**; 161:2153–67.
14. Amano S, Hazama F, Kubagawa H, Tasaka K, Haebara H, Hamashima Y. General pathology of Kawasaki disease. Acta Pathol Jpn **1980**; 30: 681–94.
15. Giesker DW, Pastuszak WT, Forouhar FA, Krause PJ, Hine P. Lymph node biopsy for early diagnosis in Kawasaki disease. Am J Surg Pathol **1982**; 6:493–501.
16. Bonany PJ, Bilkis MD, Gallo G, et al. Acute renal failure in typical Kawasaki disease. Pediatr Nephrol **2002**; 17:329–31
17. Burns JC, Wright JD, Newburger JW, et al. Conjunctival biopsy in patients with Kawasaki disease. Pediatr Pathol Lab Med **1995**; 15: 547–53.
18. Koga M, Ishihara T, Takahashi M, Umezawa Y, Furukawa S. Activation of peripheral blood monocytes and macrophages in Kawasaki disease: ultrastructural and immunocytochemical investigation. Pathol Int **1998**; 48:512–7.
19. Zhang L, Peeples ME, Boucher RC, Collins PL, Pickles RJ. Respiratory syncytial virus infection of human airway epithelial cells is polarized, specific to ciliated cells, and without obvious cytopathology. J Virol **2002**; 76:5654–66.
20. Zhang L, Bukreyev A, Thompson CI, et al. Infection of ciliated cells by human parainfluenza virus type 3 in an in vitro model of human airway epithelium. J Virol **2005**; 79:1113–24.
21. Terman A, Brunk UT. Lipofuscin: mechanisms of formation and increase with age. Acta Pathol Microbiol Immunol Scand **1998**; 106: 265–76.
22. Balakirev MY, Jaquinod M, Haas AL, Chroboczek J. Deubiquitinating function of adenovirus proteinase. J Virol **2002**; 76:6323–31.
23. Everett RD, Meredith MR, Orr A, Cross A, Kathoria M, Parkinson J. A novel ubiquitin-specific protease is dynamically associated with the PML nuclear domain and binds to a herpesvirus regulatory protein. EMBO J **1997**; 16:1519–30.
24. Sulea T, Lindner HA, Purisima EO, Menard R. Deubiquitination, a new function of the severe acute respiratory syndrome coronavirus papain-like protease? J Virol **2005**; 79:4550–1.
25. Terman A, Sandberg S. Proteasome inhibition enhances lipofuscin formation. Ann NY Acad Sci **2002**; 973:309–12.
26. Esper F, Shapiro E, Weibel C, Ferguson D, Landry ML, Kahn JS. Association between a novel human coronavirus and Kawasaki disease. J Infect Dis **2005**; 191:499–502.
27. Shimizu C, Shike H, Baker SC, et al. Human coronavirus NL63 is not detected in the respiratory tracts of children with acute Kawasaki disease. J Infect Dis **2005**; 192:000-00 (in this issue).
28. Ebihara T, Endo R, Ma X, Ishiguro N, Kikuta H. Lack of association between New Haven coronavirus and Kawasaki disease (letter). J Infect Dis **2005**; 192:351–2.
29. Belay ED, Erdman DD, Anderson LJ, et al. Kawasaki disease and human coronavirus (letter). J Infect Dis **2005**; 192:352–3.

Inflamm. res. 55 (2006) 1–7

DOI 10.1007/s00011-006-0071-3

Inflammation Research

Earlier onset of neutrophil-mediated inflammation in the ultraviolet-exposed skin of mice deficient in myeloperoxidase and NADPH oxidase

J. Komatsu[1], H. Koyama[1], N. Maeda[2] and Y. Aratani[1]

[1] Kihara Institute for Biological Research, Yokohama City University, Maioka-cho 641-12, Totsuka, Yokohama 244-0813, Japan, Fax: ++81 45 820 1901, e-mail: yaratani@yokohama-cu.ac.jp

[2] Department of Pathology and Laboratory Medicine, University of North Carolina, Chapel Hill, North Carolina 27599-7525, USA

Received 21 July 2005; returned for revision 23 December 2005; accepted by M. Parnham 23 January 2006

Abstract. *Objective and design:* This study examined the role of neutrophil-derived reactive oxygen species (ROS) in neutrophil recruitment into ultraviolet B (UVB)-exposed skin of mice.

Methods: Mouse dorsal skin was irradiated with UVB (600 mJ/cm^2). Accumulation of neutrophils within the inflammatory sites was observed histochemically. Keratinocyte-derived chemokine (KC) and macrophage inflammatory protein 2 (MIP-2) were quantified, and in vivo chemotaxis of neutrophils toward KC and MIP-2 was examined.

Results: UVB exposure of mice deficient in myeloperoxidase (MPO), NADPH oxidase, or both, caused skin neutrophil infiltration peaking at 60, 48, and 48 h, respectively, which was earlier than the 72-h peak in wild-type mice. MIP-2 level was higher in mutant than wild-type mice. Mutant neutrophils produced more MIP-2 *in vitro*. Neutrophil migration toward a localized source of KC was higher in mutant than wild-type mice. NADPH oxidase deficiency had a greater effect on migration than MPO deficiency.

Conclusions: These results suggest that ROS produced by neutrophils regulate expression of MIP-2 and migration of neutrophils toward KC. This may explain the earlier infiltration of mutant neutrophils in response to UVB.

Key words: Inflammation – Myeloperoxidase – NADPH oxidase – Neutrophil – Ultraviolet

Introduction

Neutrophils are the first line of defense against invading microorganisms such as bacteria and fungi. The most efficient microbicidal system employed by neutrophils depends on reactive oxygen species (ROS) generated by NADPH oxidase and myeloperoxidase (MPO). Patients with chronic granulomatous disease (CGD), in which granulocytes are unable to produce superoxide (O_2^-) due to deficiency in NADPH oxidase, exhibit clinical symptoms early in life, and die from recurrent infections during childhood [1, 2]. In a mouse model of X-linked CGD, infection with *Aspergillus fumigatus* results in high rates of mortality [3, 4]. We previously reported that mice deficient in MPO (MPO-KO mice) cause severe impairment in early host defense against various fungi and bacteria [5–8].

Impaired ROS production has previously been shown to cause abnormal inflammatory responses. CGD mice exhibited increased peritoneal leukocytosis in response to thioglycollate [4, 9]. Similarly, in human X-linked CGD patients, the percentage of neutrophils measured with the Rebuck skin window technique was abnormally elevated from 8 to at least 24 h after abrasion [10]. Intratracheal administration of sterilized *Aspergillus* hyphae produced a chronic bronchopneumonia with a distinctive neutrophilic infiltrate in CGD mice but not wild-type mice [3]. These studies suggest that inflammatory responses to some stimuli may be abnormal in CGD.

Ultraviolet (UV) radiation causes acute effects on the skin including sunburn. Both UVA (320–400 nm) and UVB (280–320 nm) have deleterious effects, although UVB is the more potent waveband with respect to the inflammatory response. It is well-known that neutrophils infiltrate human and murine skin following UV exposure [11–13]. There is an accumulating body of evidence demonstrating that neutrophil trafficking in inflammation is controlled by chemokines [14, 15]. In mice, the two best-defined CXC chemokines are keratinocyte-derived chemokine (KC) [16] and macrophage inflammatory protein 2 (MIP-2) [17], both of which are functional murine homologs of IL-8 and potent stimulators of neutrophil activation and tissue infiltration [15, 18]. These chemokines are also important for the mediation of UVB-induced inflammation. IL-8 is up-regulated in human keratinocytes following UVB-irradiation *in vitro* [19–21] and in vivo [13], and notably promotes neutrophilic infiltration in human skin [12].

Correspondence to: Y. Aratani

In the present study, we found that MPO and/or NADPH oxidase deficiency greatly accelerated neutrophil infiltration to the UVB-exposed site. MIP-2 was more abundantly expressed in the irradiated mutant mice. We found that mutant neutrophils produced larger amounts of MIP-2 than wild-type cells. We also found that neutrophils lacking these enzymes became more able to migrate toward a localized source of KC. These results suggest that ROS produced by neutrophils, such as $O2^-$ and hypochlorous acid (HOCl), regulate both production of MIP-2 and migration of neutrophils toward KC at sites of inflammation. This regulation by ROS provides a possible explanation for earlier infiltration of mutant neutrophils in response to UVB.

Materials and methods

Animals

Experimentation on eight- to ten-week-old female C57BL/6 mice was performed in accordance with the guidelines of Kihara Institute for Biological Research, Yokohama City University, Japan. C57BL/6 mice were purchased from Japan SLC (Hamamatsu, Japan). MPO-KO mice were generated as previously described [6] and CGD mice (gp91phox knockout; X-linked CGD) obtained from Dr. Mary C. Dinauer [4] were backcrossed at least 12 times with C57BL/6 mice to ensure similar genetic backgrounds. MPO-KO/CGD double knockout mice were generated by crossing MPO-KO with CGD mice. All animals were housed under specific-pathogen-free conditions.

Exposure of mice to UVB

Mice were anesthetized with ketamine/xylazine. The middle of the back was shaved, and the dorsal skin was irradiated with an acute (400 s), single exposure of UVB (600 mJ/cm^2) with UV lamps (UVLMS-38; Ultra-Violet Products, Upland, CA, USA) that emit predominantly UVB wavelengths (70 % of total emitted energy) with a peak emission at 302 nm. The dose of UVB was quantified with a UVB radiometer (UVX-31; Ultra-Violet Products).

Histology

The mice were sacrificed 48, 60, 72, and 96 h after UV exposure, and skin samples (3 mm long, 3 mm wide), which also contained associated dermis, were taken and placed in 4 % paraformaldehyde. Tissues for light microscopy were fixed overnight in 4 % paraformaldehyde in phosphate buffer, dehydrated in graded ethanol solutions, embedded in paraffin, sectioned at 7 µm, and stained with hematoxylin/eosin (HE). For quantification of inflammation, skin inflammation was scored in a blinded fashion by two independent investigators. A value of 0 was given when HE-stained sections showed no sign of inflammation. Sections were graded from 1 to 3 according to the severity of inflammation (1, mild; 2, moderate; and 3, severe).

For immunohistochemistry, freshly isolated tissues were frozen in dry ice using OTC compound (Sakura Finetek, Torrance, CA, USA). Sections of 10 µm were cut from the frozen tissues, dried, pre-incubated in phosphate buffered saline (PBS) containing 5 % dialyzed goat serum (Dako, Glostrup, Demmark) for 1 h, and incubated with biotinylated rat anti-Gr1 monoclonal antibody (diluted 1:200; R&D Systems, Minneapolis, MN, USA) and rabbit anti-matrix metalloproteinase-9 (MMP-9) polyclonal antibody (diluted 1:200; Chemicon, Temecula, CA, USA) overnight at 4 °C. After washing three times with PBS, the sections were incubated with secondary antibodies for 2 h at room temperature. Cy-3 conjugated streptavidin (Jackson ImmunoResearch Laboratories, West Grove, PA, USA) or FITC-conjugated anti-rabbit Ig (Chemicon) was used as the secondary antibody to visualize the primary antibody. Nuclei were stained with 4′,6′-diamidino-2-phenylindole.

Enzyme-linked immunosorbent assay (ELISA)

Freshly isolated skin samples (3 mm long, 3 mm wide) were homogenized in 0.3 ml ice-cold PBS containing 3 µl Proteinase Inhibitor Cocktail (Sigma Chemical, St. Louis, MO, USA). The homogenates were centrifuged at 3000 *g* for 20 min at 4 °C, and the resulting supernatants were frozen at –20 °C and assayed for KC using a KC-specific ELISA kit (R&D Systems) and for MIP-2 using a MIP-2-specific ELISA kit (R&D Systems) according to the manufacturer's instructions. The limit of detection of these assays was 2 and 1.5 pg/ml, respectively.

For the assay of MIP-2 production from neutrophils, peritoneal exudate cells were prepared from peritoneal cavities of mice 3 h after a single intraperitoneal injection of 1 ml 3 % fluid thioglycollate medium (Difco Laboratories, Detroit, MI, USA). Exudate cells consist of ~80 % neutrophils [22]. The cells were adjusted to 2.5×10^6 cells/ml with PBS and were activated with 30 ng/ml phorbol 12-myristate 13-acetate (PMA; Wako Chemicals, Osaka, Japan) for 1 h. Supernatants obtained by centrifugation for 5 min at 350 *g* were assayed for MIP-2 concentration as described above.

Air pouch model

The mouse air-pouch model for in vivo chemotaxis has been described in detail elsewhere [23–25]. On experimental day 0, 2.5 ml sterile air was injected under the dorsal skin to raise subcutaneous (s.c.) air pouches; the resultant space was reinjected with 2.5 ml sterile air on day 3. On day 6, 0.5 µg recombinant KC (R&D Systems) or 0.2 µg recombinant MIP-2 (R&D Systems) dissolved in 1 ml PBS was injected into the pouch cavities. The animals were sacrificed 2 h later, and the pouch exudates were harvested by washing the s.c. cavities three times with 2 ml ice-cold PBS containing 3 mM EDTA. The resulting cell suspensions were centrifuged at 350 *g* for 10 min at 4 °C, and the cell pellets were re-suspended in 0.1 ml PBS. The numbers of leukocytes per pouch were calculated from differential cell counts of 0.1 ml re-suspended cells diluted fourfold (v/v) in Turk solution (0.01 % crystal violet w/v in 3 % acetic acid; Nakaraitesk, Kyoto, Japan) using a hemocytometer. Recruited cells were defined as polymorphonuclear or mononuclear leukocytes, and polymorphonuclear leukocytes were considered to be neutrophils. The absolute number of neutrophils in each sample was determined by multiplying the percentage of this cell type by the total number of leukocytes per sample.

Statistics

Data were analyzed and expressed as mean ±SD. Statistical analysis was performed using one-way ANOVA with Bonferroni correction for multiple comparisons. Probability values were considered statistically significant at <0.05.

Results

MPO and NADPH oxidase deficiency shows earlier skin inflammation in response to UVB exposure

Irradiation of shaved dorsal skin with UVB light induced transient inflammation in the dermis and epidermis. In wild-type mice, no obvious inflammation was observed 48 h after irradiation (Figs. 1A and B). Inflammation peaked at 72 h, and returned to the control level at 96 h (Fig. 1B). In MPO-KO mice, it is of interest that a maximum accumulation of inflammatory cells was observed at 60 h (Fig. 1B), which

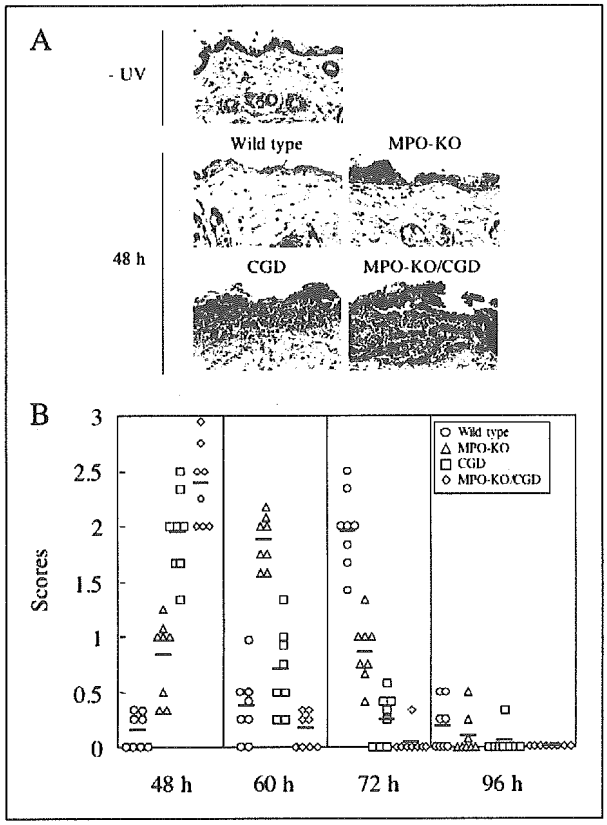

Fig. 1. Histopathology of dorsal skin sections from UVB-irradiated mice. Mice of the indicated genotypes were exposed to UVB and the dorsal skin sections were prepared at the indicated times postirradiation. (A) Representative photomicrographs (×40) of HE-stained sections at 48 h after irradiation. A skin section not irradiated with UVB (–UV) was also stained with HE as a control. (B) Inflammation scores on histology sections. The severity of inflammation was determined in a blinded fashion on a 4-point scale (0, minimal inflammation; 3, massive inflammation). Values shown are means based on three measurements per histological section in five histological sections per mouse. Bars indicate mean scores determined from the severity of eight mice in each time point.

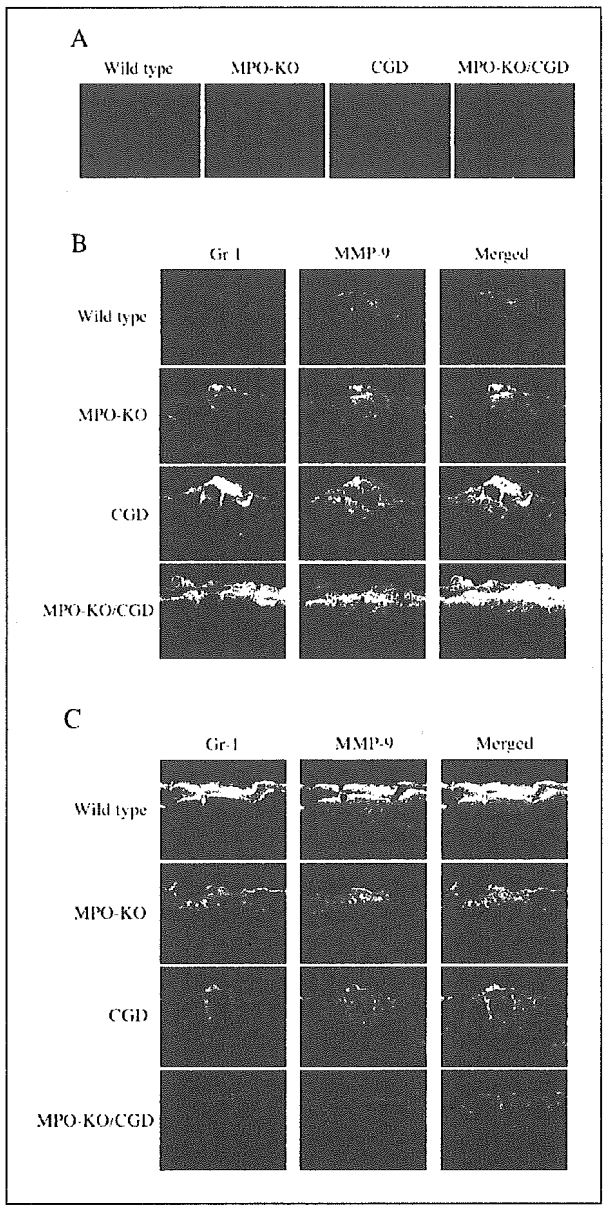

Fig. 2. Tissue sections showing neutrophil infiltration in the skin of mutant and wild-type mice 48 h (B) and 72 h (C) after UVB-irradiation. Neutrophils were stained with anti-Gr-1 antibody (red) and anti-MMP-9 antibody (green). Skin sections not irradiated with UVB were also stained with Gr-1 as controls (A). Data shown are representative of five mice with each genotype. Original magnification, ×40.

is considerably earlier than in wild-type mice. In CGD and MPO-KO/CGD mice, inflammation proceeded more rapidly; a peak was observed at 48 h (Figs. 1A and B), and a regular reconstitution of epithelial layers was observed 72 h postirradiation (data not shown). Inflammation observed in the MPO-KO/CGD mice at 48 h was more severe than that in the CGD mice. No inflammation was observed at 24 h in any of the mice, regardless of genotype (data not shown). These results indicate that lack of MPO and/or NADPH oxidase results in an earlier onset of inflammation, and that the effect of NADPH oxidase deficiency is more pronounced than that of MPO deficiency.

UV irradiation induces neutrophil infiltration

Although a variety of leukocytes migrate outside blood vessels and infiltrate UVB-exposed sites, neutrophils are the main infiltrating cells in the inflammatory phase [11, 26]. Infiltration of Gr-1-positive neutrophils was assessed immunohistochemically. Gr-1-positive neutrophils were rarely detected in any of the mice with different genotypes before UVB treatment (Fig. 2A). At 48 h after irradiation (Fig. 2B), neutrophils were still not detected in the wild-type mice. In contrast, a slight accumulation of neutrophils was observed, mostly in the epidermis, of MPO-KO mice, and a larger accumulation in the dermis and epidermis was observed

in CGD mice. The deficiency of both MPO and NADPH oxidase caused the largest accumulation at 48 h. In wild-type mice, neutrophil infiltration reached a maximum at 72 h, whereas most of the neutrophils had already disappeared in the CGD and MPO-KO/CGD mice by this time (Fig. 2C). The time course of neutrophil accumulation in each genotype was associated with the severity of inflammation observed in Figure 1, indicating that the majority of inflammatory cells were neutrophils.

Neutrophils are producers of proteolytic enzymes including MMP-9 [27]. Sections from skin were double-stained for MMP-9 and Gr-1. Some MMP-9-positive cells co-localized with Gr-1-positive cells (Fig. 2B and C), indicating that a proportion of the MMP-9-expressing cells was in fact accumulated neutrophils at the UV-exposed site. These results suggest that earlier neutrophil infiltration is capable of inflicting earlier tissue damage in the skin.

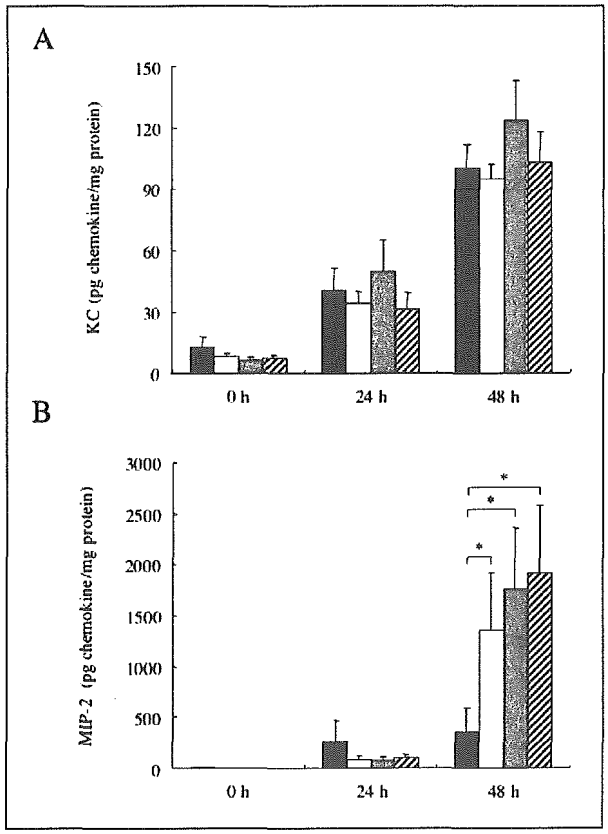

Fig. 3. Production of KC and MIP-2 in the skin of wild-type, MPO-KO, CGD, and MPO-KO/CGD mice after UVB-exposure. Skin tissues were collected at different time points from wild-type (black bars), MPO-KO (white bars), CGD (gray bars), and MPO-KO/CGD (hatched bars) mice. KC (A) and MIP-2 (B) levels were measured using specific ELISAs. The detection limits of the assays were 2 and 1.5 pg/ml, respectively. The data are the mean±SD of the results from five different mice. *, $P < 0.05$, compared to wild-type mice.

KC and MIP-2 generation in UVB-exposed skin

KC and MIP-2 are well-defined CXC chemokines controlling neutrophil recruitment. To address the mechanism by which neutrophils deficient in MPO and/or NADPH oxidase more rapidly emigrate into the skin in response to UVB irradiation, we measured the amounts of KC and MIP-2 in skin homogenates. Both chemokine levels were significantly and time-dependently elevated during the 48 h after UVB exposure (Fig. 3A and B), suggesting that these chemokines contribute to neutrophil recruitment. However, there was no significant difference in the KC level between the mice with different genotypes at each time point (Fig. 3A). In contrast, it should be noted that the MIP-2 level at 48 h was significantly higher in all of the mutant mice compared to the wild type (Fig. 3B). Although MIP-2 level in CGD and MPO-KO/CGD mice was slightly higher than in MPO-KO mice, it was not significantly different. Therefore, it is possible that the earlier recruitment of neutrophils in mutant mice is dependent on MIP-2 expression, but independent of KC expression.

MIP-2 production by neutrophils in vitro

The amount of MIP-2 produced from neutrophils was determined by specific ELISA. Peritoneal exudate neutrophils rarely produced MIP-2 irrespective of mouse genotype (Fig. 4). Notably, however, we found that stimulation of neutrophils from MPO-KO or CGD mice with PMA resulted in an increase in MIP-2 production, which was significantly greater than that seen in normal neutrophils. Although not significant, neutrophils from MPO-KO/CGD mice produced a larger amount of MIP-2 than those from the single mutant mice. These results indicate that neutrophil-derived ROS regulate the production of MIP-2 from neutrophils.

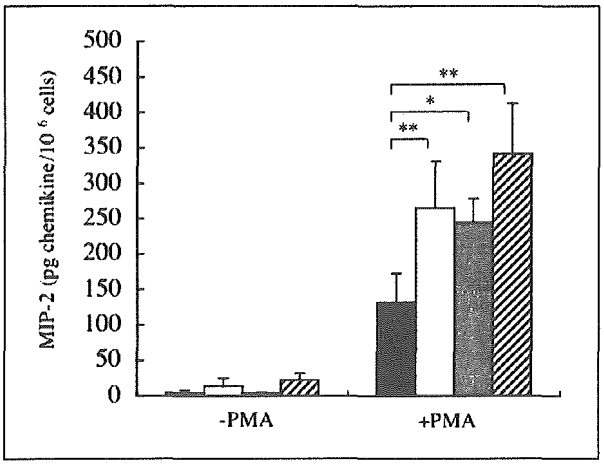

Fig. 4. Production of MIP-2 from neutrophils in vitro. Peritoneal exudate cells were prepared from wild-type (black bars), MPO-KO (white bars), CGD (gray bars), and MPO-KO/CGD (hatched bars) mice. The cells (2.5×10^6 cells/ml) were incubated with (+) or without (–) PMA (30 ng/ml) for 1 h. MIP-2 levels of four mice with each genotype were determined by ELISA. The data are the mean ±SD. *, $P < 0.05$; **, $P < 0.01$.

KC-induced neutrophil recruitment is regulated by MPO and/or NADPH oxidase

Injection of KC into air pouches caused a dramatic, neutrophil-dominated (>85%) leukocyte response. As shown in Figure 5A, the number of exudate neutrophils 2h after KC injection in the pouches of MPO-KO mice was 1.9-fold higher than that in the pouches of wild-type mice. Compared to the MPO-KO mice, a larger number of CGD neutrophils infiltrated, and the largest number of neutrophils was recovered from the MPO-KO/CGD mice. The number of neutrophils from the air pouches obtained by injection of vehicle alone was $<0.5 \pm 0.1 \times 10^5$ cells/pouch.

We also examined MIP-2-provoked neutrophil recruitment (Fig. 5B), but no significant difference was observed between the wild type and any of the mutant mice. These results indicate that neutrophils lacking ROS production due to MPO and/or NADPH-oxidase deficiency become more able to migrate toward a localized source of KC, and suggest that this response to KC may contribute, at least in part, to the earlier infiltration of CGD and MPO-KO neutrophils in response to UVB.

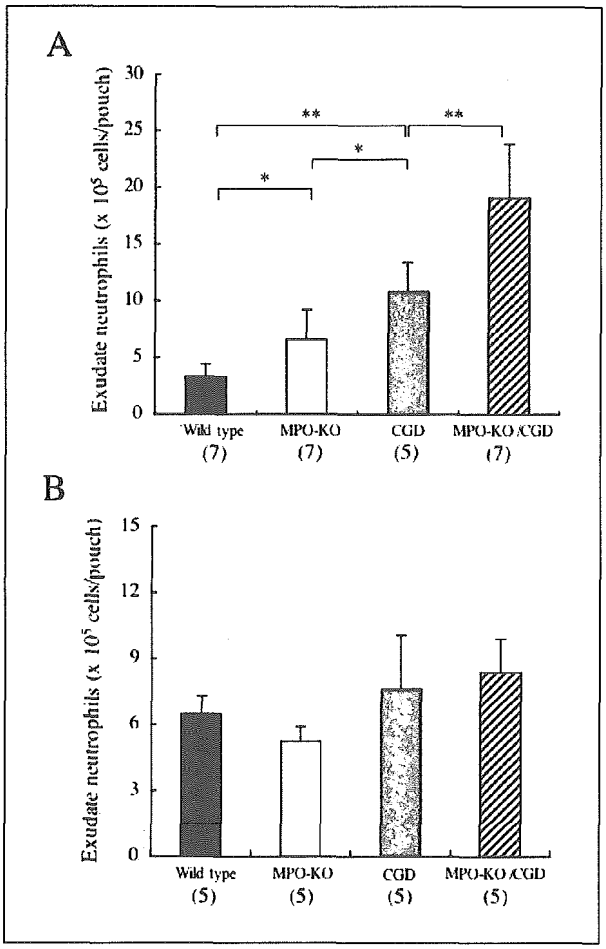

Fig. 5. Greater migrating activity of neutrophils deficient in MPO and/or NADPH oxidase toward KC in vivo. PBS containing recombinant KC (A) or MIP-2 (B) was injected into air pouches generated on the back of wild-type (black bars), MPO-KO (white bars), CGD (gray bars), and MPO-KO/CGD (hatched bars) mice. The number of neutrophils exuded in the pouch was determined 2h after injection. The data are the mean±SD. The number in parentheses indicates the number of mice used in each assay. *, $P < 0.05$; **, $P < 0.01$.

Discussion

This paper describes the involvement of MPO and NADPH oxidase in the UVB-responsive recruitment of neutrophils. Our data demonstrate that lack of MPO and/or NADPH oxidase results in an earlier onset of inflammation accompanied by neutrophil infiltration in response to UVB-exposure. CGD mice showed earlier infiltration of neutrophils than MPO-KO mice (Fig. 2), indicating that O_2^- or its metabolites produced by NADPH oxidase regulates neutrophil infiltration more strongly than HOCl. This inflammatory response in the mutant mice was associated with an increase in MIP-2 level produced by skin exposed to UVB (Fig. 3B). It was also associated with a significant increase in the migration of neutrophils toward a localized source of KC (Fig. 5A). These results suggest that MPO and NADPH oxidase are responsible for the development of UVB-induced skin inflammation, possibly by up-regulating both expression of MIP-2 in response to UVB and KC-dependent neutrophil migration.

Leukocyte recruitment to sites of inflammation is regulated by chemokines. To understand the mechanism by which neutrophils deficient in MPO and/or NADPH oxidase accumulate earlier at UVB-exposed sites, we first determined the concentration of chemokines expressed in the skin. KC is a key mediator of acute recruitment of neutrophils [15, 18]. Our data showed a significant increase in KC level following UVB exposure of the dorsal skin of mice, consistent with a previous report that IL-8 is up-regulated in the epidermis of normal human skin after UVB exposure [13]. However, no significant difference in the level of KC was detected between any the mice regardless of genotype (Fig. 3A), indicating that earlier neutrophil accumulation is independent of endogenous KC expression.

MIP-2 is another key mediator of neutrophil recruitment. We found that MIP-2 level in all mutant mice was significantly higher than that in wild-type mice (Fig. 3B), suggesting that the larger amount of MIP-2 is at least partly involved in the earlier infiltration of neutrophils to skin exposed to UVB. Several cell types including macrophages [28], epithelial cells [29], mast cells [30], and neutrophils [31–33] have been identified as sources of MIP-2. Notably, we found that mutant neutrophils produced larger amounts of MIP-2 than wild-type neutrophils in vitro when stimulated with PMA (Fig. 4). The data indicate that MPO and/or NADPH oxidase deficiency up-regulates the production of MIP-2 from neutrophils. Since an early release of MIP-2 can promote recruitment of more neutrophils, greater production of this chemokine from the mutant neutrophils provides a possible explanation for the earlier accumulation of neutrophils in the skin of mutant mice in response to UVB.

The s.c. air pouch has been used extensively as a model of leukocyte extravasation in vivo [23, 25, 34]. The advantage of this model is that leukocytes migrating into the pouch

in response to inflammatory mediators can be collected and counted. In the present study, we used this model to examine the migration rate of each neutrophil in mice with different genotypes toward KC and MIP-2. Injection of KC and MIP-2 into the pouch induced a rapid (2 h) accumulation of neutrophils (Fig. 5), confirming that both chemokines are critical mediators of neutrophil accumulation in acute inflammation. Surprisingly, we also found that neutrophil migration toward KC was higher in mutant than wild-type mice (Fig. 5A). The greater migrating activity of those neutrophils toward endogenously expressed KC may have been involved in the earlier neutrophil recruitment in the mutant mice in response to UVB. Neutrophil migration to KC is mediated through its receptor CXCR2 [35, 36]. To further understand how neutrophil-derived ROS regulate migration of neutrophils toward KC, we measured surface expression of CXCR2 on the air pouch-exudate neutrophils. However, flow cytometry revealed that there was no significant difference in the expression level between mice with different genotypes (data not shown). Therefore, it is not likely that neutrophil-derived ROS regulate the number of CXCR2. In contrast, neutrophils with different genotypes showed an equivalent response to a localized source of MIP-2 (Fig. 5B), suggesting that neither neutrophil-derived O_2^- nor HOCl regulates the migration of neutrophils toward MIP-2.

The acute inflammatory state normally represents a transient proteolytic episode that gives way to phases of remodeling and tissue regeneration. Neutrophils are potent producers of a wide array of proteolytic enzymes, including MMP-9, which is potentially capable of inflicting serious extracellular matrix damage [27]. In the skin, MMP-9 is generally associated with keratinocytes and fibroblasts. However, our data indicate that UVB irradiation elevates MMP-9 protein levels by recruiting neutrophils containing MMP-9 in mouse skin in vivo, consistent with a recent report of UV-irradiated human skin [37]. Taken together, it is likely that the earlier accumulation of neutrophils causes earlier tissue destruction followed by tissue regeneration.

Although further studies are necessary to clarify the mechanism by which neutrophils deficient in O_2^- and HOCl production accumulate more rapidly at UVB-exposed sites, our present findings strongly suggest that neutrophil-derived ROS are factors that control neutrophil infiltration to inflammatory sites.

Acknowledgements. We thank Dr. Mary C. Dinauer, Indiana University School of Medicine, for kindly providing the CGD mice. We also thank Aya Kurosawa and Chie Nishigaki for technical support, and Ayako Onuma for animal care. This work was supported in part by Grants-in-Aid from the Ministry of Education, Culture, Sports, Science and Technology and from the Japan Health Sciences Foundation.

References

[1] Dinauer MC. The respiratory burst oxidase and the molecular genetics of chronic granulomatous disease. Crit Rev Clin Lab Sci 1993; 30: 329–69.
[2] Gallin JI, Buescher ES, Seligmann BE, Nath J, Gaither T, Katz P. NIH conference. Recent advances in chronic granulomatous disease. Ann Intern Med 1983; 99: 657–74.
[3] Morgenstern DE, Gifford MA, Li LL, Doerschuk CM, Dinauer MC. Absence of respiratory burst in X-linked chronic granulomatous disease mice leads to abnormalities in both host defense and inflammatory response to Aspergillus fumigatus. J Exp Med 1997; 185: 207–18.
[4] Pollock JD, Williams DA, Gifford MA, Li LL, Du X, Fisherman J et al. Mouse model of X-linked chronic granulomatous disease, an inherited defect in phagocyte superoxide production. Nat Genet 1995; 9: 202–9.
[5] Aratani Y, Kura F, Watanabe H, Akagawa H, Takano Y, Suzuki K et al. Critical role of myeloperoxidase and nicotinamide adenine dinucleotide phosphate-oxidase in high-burden systemic infection of mice with Candida albicans. J Infect Dis 2002; 185: 1833–7.
[6] Aratani Y, Koyama H, Nyui S, Suzuki K, Kura F, Maeda N. Severe impairment in early host defense against Candida albicans in mice deficient in myeloperoxidase. Infect Immun 1999; 67: 1828–36.
[7] Aratani Y, Kura F, Watanabe H, Akagawa H, Takano Y, Suzuki K et al. Differential host susceptibility to pulmonary infections with bacteria and fungi in mice deficient in myeloperoxidase. J Infect Dis 2000; 182: 1276–9.
[8] Aratani Y, Kura F, Watanabe H, Akagawa H, Takano Y, Suzuki K et al. Relative contributions of myeloperoxidase and NADPH-oxidase to the early host defense against pulmonary infections with Candida albicans and Aspergillus fumigatus. Med Mycol 2002; 40: 557–63.
[9] Jackson SH, Gallin JI, Holland SM. The p47phox mouse knock-out model of chronic granulomatous disease. J Exp Med 1995; 182: 751–8.
[10] Gallin JI, Buescher ES. Abnormal regulation of inflammatory skin responses in male patients with chronic granulomatous disease. Inflammation 1983; 7: 227–32.
[11] Hawk JL, Murphy GM, Holden CA. The presence of neutrophils in human cutaneous ultraviolet-B inflammation. Br J Dermatol 1988; 118: 27–30.
[12] Cooper KD, Duraiswamy N, Hammerberg C, Allen E, Kimbrough-Green C, Dillon W et al. Neutrophils, differentiated macrophages, and monocyte/macrophage antigen presenting cells infiltrate murine epidermis after UV injury. J Invest Dermatol 1993; 101: 155–63.
[13] Strickland I, Rhodes LE, Flanagan BF, Friedmann PS. TNF-alpha and IL-8 are upregulated in the epidermis of normal human skin after UVB exposure: correlation with neutrophil accumulation and E-selectin expression. J Invest Dermatol 1997; 108: 763–8.
[14] Ebnet K, Vestweber D. Molecular mechanisms that control leukocyte extravasation: the selectins and the chemokines. Histochem Cell Biol 1999; 112: 1–23.
[15] Rollins BJ. Chemokines. Blood 1997; 90: 909–28.
[16] Cochran BH, Reffel AC, Stiles CD. Molecular cloning of gene sequences regulated by platelet-derived growth factor. Cell 1983; 33: 939–47.
[17] Tekamp-Olson P, Gallegos C, Bauer D, McClain J, Sherry B, Fabre M et al. Cloning and characterization of cDNAs for murine macrophage inflammatory protein 2 and its human homologues. J Exp Med 1990; 172: 911–9.
[18] Zlotnik A, Morales J, Hedrick JA. Recent advances in chemokines and chemokine receptors. Crit Rev Immunol 1999; 19: 1–47.
[19] Kondo S, Kono T, Sauder DN, McKenzie RC. IL-8 gene expression and production in human keratinocytes and their modulation by UVB. J Invest Dermatol 1993; 101: 690–4.
[20] Pernet I, Sagot V, Schmitt D, Viac J. UVA1 and UVB radiation but not PGE2 stimulate IL-8 release in normal human keratinocytes. Arch Dermatol Res 1999; 291: 527–9.
[21] Stein M, Bernd A, Ramirez-Bosca A, Kippenberger S, Holzmann H. Measurement of anti-inflammatory effects of glucocorticoids on human keratinocytes in vitro. Comparison of normal human keratinocytes with the keratinocyte cell line HaCaT. Arzneimittelforschung 1997; 47: 1266–70.
[22] Tsurubuchi T, Aratani Y, Maeda N, Koyama H. Retardation of early-onset PMA-induced apoptosis in mouse neutrophils deficient in myeloperoxidase. J Leukoc Biol 2001; 70: 52–8.
[23] Edwards JC, Sedgwick AD, Willoughby DA. The formation of a structure with the features of synovial lining by subcutaneous injection of air: an in vivo tissue culture system. J Pathol 1981; 134: 147–56.

[24] Liu Q, Wang Y, Thorlacius H. Dexamethasone inhibits tumor necrosis factor-alpha-induced expression of macrophage inflammatory protein-2 and adhesion of neutrophils to endothelial cells. Biochem Biophys Res Commun 2000; 271: 364–7.
[25] Schramm R, Schaefer T, Menger MD, Thorlacius H. Acute mast cell-dependent neutrophil recruitment in the skin is mediated by KC and LFA-1: inhibitory mechanisms of dexamethasone. J Leukoc Biol 2002; 72: 1122–32.
[26] Norris P, Poston RN, Thomas DS, Thornhill M, Hawk J, Haskard DO. The expression of endothelial leukocyte adhesion molecule-1 (ELAM-1), intercellular adhesion molecule-1 (ICAM-1), and vascular cell adhesion molecule-1 (VCAM-1) in experimental cutaneous inflammation: a comparison of ultraviolet B erythema and delayed hypersensitivity. J Invest Dermatol 1991; 96: 763–70.
[27] Opdenakker G, Van den Steen PE, Dubois B, Nelissen I, Van Coillie E, Masure S et al. Gelatinase B functions as regulator and effector in leukocyte biology. J Leukoc Biol 2001; 69: 851–9.
[28] Wolpe SD, Sherry B, Juers D, Davatelis G, Yurt RW, Cerami A. Identification and characterization of macrophage inflammatory protein 2. Proc Natl Acad Sci U S A 1989; 86: 612–6.
[29] Zhao MQ, Stoler MH, Liu AN, Wei B, Soguero C, Hahn YS et al. Alveolar epithelial cell chemokine expression triggered by antigen-specific cytolytic CD8(+) T cell recognition. J Clin Invest 2000; 106: R49–58.
[30] Biedermann T, Kneilling M, Mailhammer R, Maier K, Sander CA, Kollias G et al. Mast cells control neutrophil recruitment during T cell-mediated delayed-type hypersensitivity reactions through tumor necrosis factor and macrophage inflammatory protein 2. J Exp Med 2000; 192: 1441–52.
[31] Hang L, Haraoka M, Agace WW, Leffler H, Burdick M, Strieter R et al. Macrophage inflammatory protein-2 is required for neutrophil passage across the epithelial barrier of the infected urinary tract. J Immunol 1999; 162: 3037–44.
[32] Greenberger MJ, Strieter RM, Kunkel SL, Danforth JM, Laichalk LL, McGillicuddy DC et al. Neutralization of macrophage inflammatory protein-2 attenuates neutrophil recruitment and bacterial clearance in murine Klebsiella pneumonia. J Infect Dis 1996; 173: 159–65.
[33] Matzer SP, Baumann T, Lukacs NW, Rollinghoff M, Beuscher HU. Constitutive expression of macrophage-inflammatory protein 2 (MIP-2) mRNA in bone marrow gives rise to peripheral neutrophils with preformed MIP-2 protein. J Immunol 2001; 167: 4635–43.
[34] Tessier PA, Naccache PH, Clark-Lewis I, Gladue RP, Neote KS, McColl SR. Chemokine networks in vivo: involvement of C-X-C and C-C chemokines in neutrophil extravasation in vivo in response to TNF-alpha. J Immunol 1997; 159: 3595–602.
[35] Lee J, Cacalano G, Camerato T, Toy K, Moore MW, Wood WI. Chemokine binding and activities mediated by the mouse IL-8 receptor. J Immunol 1995; 155: 2158–64.
[36] Cacalano G, Lee J, Kikly K, Ryan AM, Pitts-Meek S, Hultgren B et al. Neutrophil and B cell expansion in mice that lack the murine IL-8 receptor homolog. Science 1994; 265: 682–4.
[37] Rijken F, Bruijnzeel PL, van Weelden H, Kiekens RC. Responses of black and white skin to solar-simulating radiation: differences in DNA photodamage, infiltrating neutrophils, proteolytic enzymes induced, keratinocyte activation, and IL-10 expression. J Invest Dermatol 2004; 122: 1448–55.

Journal of Chemical Engineering of Japan, Vol. 38, No. 4, pp. 295–299, 2005 **Research Paper**

Condensation Reactions of Amino Acids under Hydrothermal Conditions with Adiabatic Expansion Cooling

Tomomasa GOTO[1], Yasuhiro FUTAMURA[2,3], Yukio YAMAGUCHI[1] and Kenji YAMAMOTO[1,2]

[1]*Department of Chemical System Engineering, Graduate School of Engineering, The University of Tokyo, 3-1, Hongo 7, Bunkyou-ku, Tokyo 113-8656, Japan*

[2]*Department of Medical Ecology and Informatics, Research Institute, International Medical Center of Japan, 21-1, Toyama 1, Shinjuku-ku, Tokyo 162-8655, Japan*

[3]*Department of Bioactive Molecules, The National Institute of Infectious Diseases, 23-1, Toyama 1, Shinjuku-ku, Tokyo 162-8640, Japan*

Keywords: Peptide Polymerization, Adiabatic Expansion, Hydrothermal System, Prevention from Hydrolysis Reaction, Origin of Life

A novel flow reactor adopted for the adiabatic expansion cooling method, a rapid quenching method, was designed to synthesize oligopeptides from amino acids under hydrothermal conditions. We studied the hydrothermal reaction under the two experimental conditions, whose raw materials were glycine and diglycine aqueous solution. The temperature, the pressure and the residence time of the reaction were 270°C, 10 MPa and 27 seconds, respectively. Then we could obtain long oligoglycines like octa-, nona- and decaglycine. The concentration profiles of each product in the two experimental conditions were similar. It suggests that the equilibrium relations would be established between condensation reactions and hydrolysis reactions of oligoglycines, which might light up a new pathway to the study of the origin of life.

Introduction

We designed a novel flow reactor for synthesizing oligopeptides from amino acids in subcritical and supercritical water. In this reactor the method for quenching the solution after the reaction was adopted for the adiabatic expansion. We hypothesized that the method for quenching the solution had to be so rapid that we could obtain long oligopeptides. Shock (1992) reported that the thermodynamic equilibrium would shift to the condensation of amino acids as the temperature increased. This report suggests that the rapid quenching, a non-equilibrium method, could avoid hydrolysis and dissociation of the oligopeptides, which had already been synthesized under hydrothermal conditions. In short, the rapid quenching method such as the adiabatic expansion made it feasible that the oligopeptides were brought into our hands at room temperature and the atmospheric pressure. Here, the abundance ratio of products was kept at the equilibrium between condensation and hydrolysis of oligopeptides at high temperature and high pressure.

Several studies suggest the importance of quenching speed (Imai *et al.*, 1999; Ogata *et al.*, 2000; Alargov *et al.*, 2002; Islam *et al.*, 2003). In the study of Ogata *et al.* (2000) the method for cooling after the reaction that had been already heated at 250°C and pressurized at 24 MPa, was to pour the solution into a cold water bath whose pressure was somewhat higher than the atmospheric pressure. They found that di-, tri- and hexaglycine were synthesized from glycine without adding metal ions. Both Islam *et al.* (2003) and Alargov *et al.* (2002) applied another method to quenching the solution. After the glycine aqueous solution reacted at high temperature and high pressure, it passed through a cooling tube, the outside of which was bathed in cold water. However, the two research groups failed in synthesizing longer peptides like hexaglycine although their reaction conditions, the temperature and the pressure, were similar to those in the study of Ogata *et al.* (2000). The quenching method was supposed to play a key role in making their results differ greatly from each other. In fact, the method of pouring the solution into

Received on November 11, 2004. Correspondence concerning this article should be addressed to K. Yamamoto (E-mail address: backen@ri.imcj.go.jp).

Partly presented at the 36th Autumn Meeting of the Society of Chemical Engineers, Japan, at Sendai, September 2003, at the 10th Asian Pacific Confederation of Chemical Engineering, Japan, at Kitakyushu, October 2004, and at the 70th Annual Meeting of the Society of Chemical Engineers, Japan, at Nagoya, March 2005.

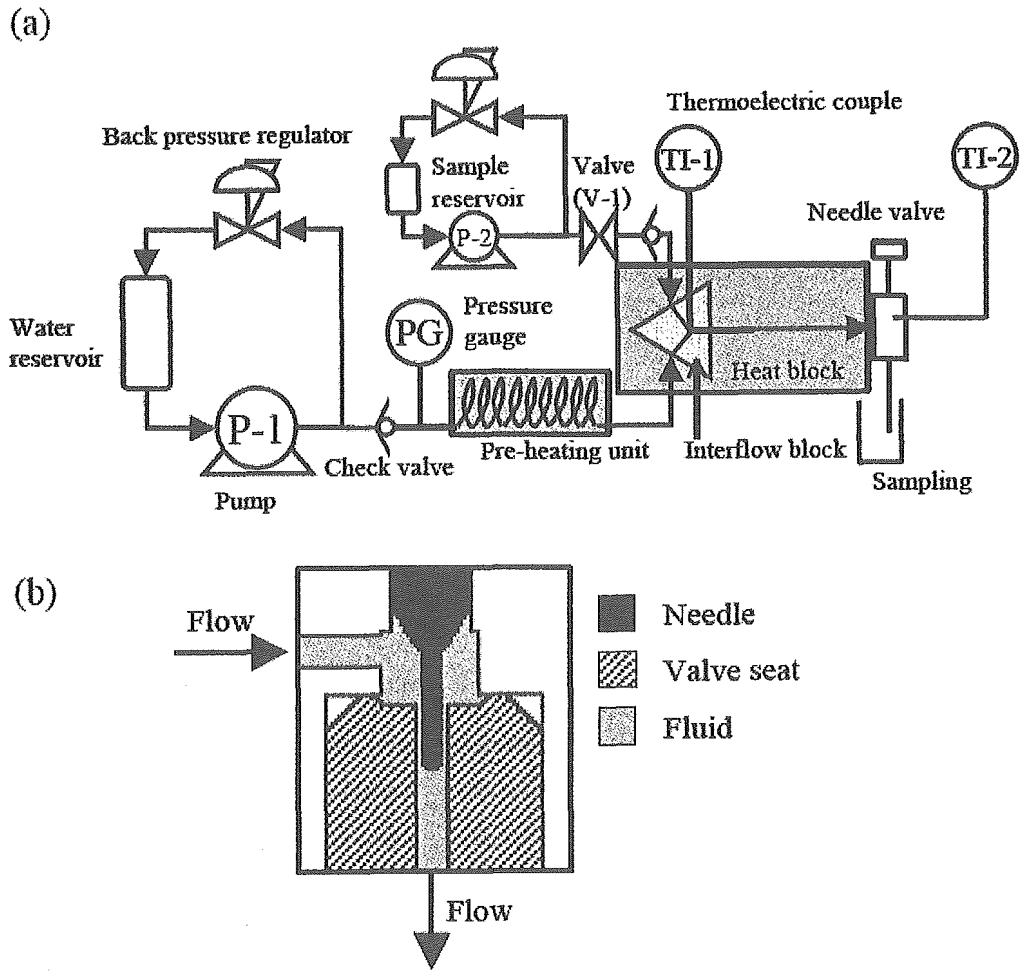

Fig. 1 (a) The experimental apparatus adopted for the adiabatic expansion cooling with a needle valve to reduce the hydrolysis reaction of the products; This flow reactor was designed to endure up to 40 MPa and 500°C. Almost all the parts that contacted with the solution were made of stainless steel SUS316. A stainless tube, by which a heat block kept heated, was placed between an interflow block and an inlet of a needle valve. The volume of the tube was 1.5 mL. (b) The detailed view inside the needle valve; the needle was attached to a valve seat and there was a very small gap between the needle and the valve seat. The pressure of the reactor was controlled with two back pressure regulators and the needle valve

the cold bath more rapidly resulted in the synthesis of the longer oligoglycine.

The adiabatic expansion cooling was thought to be one of the most rapid methods for quenching the solution. When the solution that had reacted at high temperature and high pressure was erupted into the atmosphere through the needle valve, it was both depressurized and cooled quickly with the Joule-Thomson effect. We used this method to reduce the decomposition of products. In this paper we demonstrated that the adiabatic expansion cooling method was an appropriate one to obtain the longer peptide and the equilibrium relation between condensation and hydrolysis of oligoglycines under hydrothermal conditions would be established.

1. Experimental

The flow diagram of the experimental apparatus we designed is shown in **Figure 1(a)**. This flow reactor was designed to endure high pressure and high temperature, up to 40 MPa and 500°C respectively. Almost all the parts that contacted with solution were made of stainless steel SUS316. The apparatus had two reservoirs, one was for water and the other was for the sample solution. Water was pressurized by the pump P-1 (NP-KX-500-20; Nihon Seimitsu Kagaku Co., Ltd.) and was heated with the pre-heating unit. On the other hand, the pump P-2 (NP-D-324; Nihon Seimitsu Kagaku Co., Ltd.) pressurized the sample solution. In order to raise the temperature of the sample solution rapidly, the sample solution and heated water were mixed together in the interflow block whose temperature was monitored with a thermoelectric couple

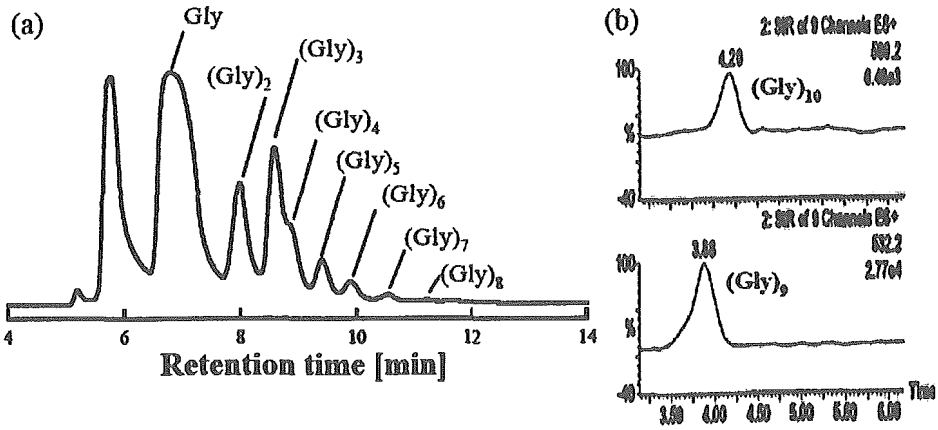

Fig. 2 (a) An high performance liquid chromatography (HPLC) profile of the products in the sample that reacted from 1.0 M glycine aqueous solution at 270°C and 10 MPa. (b) Selected Ion Monitoring (SIM) chromatograms of decaglycine (top) and nonaglycine (bottom); $(Gly)_i$ denotes the i-mer of glycine. The profile and the chromatograms were obtained from the HPLC system and the LC/MS system respectively, with the use of the same reverse-phased column (Waters Xterra MS C_{18} 2.5 mm; 4.6 × 50 mm). An aqueous solution of 50 mM KH_2PO_4 within 7.2 mM $C_6H_{13}SO_3Na$ (pH = 2.5) was used as a mobile phase in the condition for (a). The UV detector monitored the absorbance at 200 nm. In the condition for (b), an aqueous solution of 1 mM $C_5F_{11}COOH$ was used as a mobile phase and the oligoglycines were detected in the Selected Ion Recording (SIR) mode

(TD-11S; SHIMADEN Co., Ltd.). A stainless tube, by which the heat block kept heated, was placed between the interflow block and the inlet of a needle valve. The volume of the tube where material would react was 1.5 mL. Figure 1(b) is the details of the inside of the needle valve. The needle was connected with the valve seat and there was a very small gap between the needle and the valve seat. The pressure of the reactor was controlled with two back pressure regulators and the needle valve. To keep the solution heated just before adiabatic expansion cooling, the needle valve was also kept heated. The needle valve made it feasible that the solution was quenched more rapidly than by a water-cooling unit, a conventional method. Therefore it was expected that hydrolysis or decomposition of the products would be suppressed during quenching and depressurizing the solution.

We analyzed the products in an aqueous solution with a high performance liquid chromatography, HPLC, (600E Multisolvent Delivery System and 2487 Dual λ absorbance Detector; Waters Co.) to identify and quantify oligoglycines. A reverse-phased column (Waters Xterra MS C_{18} 2.5 mm; 4.6 × 50 mm) was applied and an aqueous solution of 50 mM KH_2PO_4 within 7.2 mM $C_6H_{13}SO_3Na$ (pH = 2.5) was used as a mobile phase (Tucker *et al.*, 1989). The flow rate of the mobile phase was 0.5 mL/min and the UV detector monitored the absorbance at 200 nm. We also used a Liquid chromatography/Mass spectrometer system, LC/MS, (2695 separation module and Micromass ZQ2000 mass spectrometer; Waters Co.) in order to identify too long oligoglycines to be available as a standard, like nonaglycine and decaglycine. The column was the reverse-phased column as described above and the mobile phase was an aqueous solution of 1 mM $C_5F_{11}COOH$ (Pearson and McCroskey, 1996). Oligoglycines were detected in the Selected Ion Recording mode.

Glycine, glycine anhydride and 1-hexane sulfonic acid sodium salt were purchased from Wako Pure Chemical Industries, Ltd. Diglycine, triglycine, tetraglycine, pentaglycine, hexaglycine, Phosphoric acid and Potassium dihydrogen phosphate were purchased from Sigma-Aldrich Co. Heptaglycine and octaglycine were purchased from Invitrogen Co. The purified water was from Kozakai Seiyaku Co., Ltd. Undecafluorohexaonic acid was purchased from Tokyo Kasei Kogyo Co., Ltd.

2. Results and Discussion

Water was heated to nearly 500°C in the pre-heating unit and was pressurized at 10 MPa by the pump P-1 whose flow rate was 1.3 mL/min. At the same time, sample solutions, 2.0 M glycine and 1.5 M diglycine aqueous solutions, were put into the sample reservoir and was pressurized by the pump P-2 whose rate was also 1.3 mL/min because the concentration of the glycine and diglycine solution after the mixing in the interflow block would be 1.0 M and 0.75 M respectively. Considering the density of water at 270°C and 10 MPa, the residence time of the reaction was always 27 seconds. With the rate of the input being 2.6 mL/min, the needle valve was controlled so that its rate of the output would be about 2.6 mL/min. Moreover, both the heat block and the needle valve were heated to the

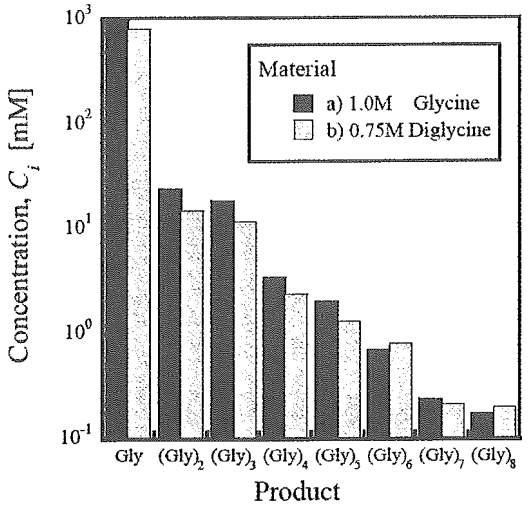

Fig. 3 The concentration profiles of the products in the two samples that obtained from (a) 1.0 M glycine and (b) 0.75 M diglycine aqueous solutions at 270°C and 10 MPa without the compensation by the concentration in erupting and expanding; $(Gly)_i$ denotes the i-mer of glycine

reaction temperature of 270°C. After the reaction in highly heated and highly pressurized water, the solution was rapidly quenched and depressurized by the needle valve.

We have sampled reaction solutions at the outlet of the needle valve in two kinds of experiments whose raw material was 1.0 M glycine and 0.75 M diglycine aqueous solution respectively. The samples had been already concentrated about three times because of erupting and expanding to the open system. We analyzed the two samples with the HPLC system to identify and quantify their products. **Figure 2(a)** shows an HPLC profile of the products in the solution that obtained from 1.0 M glycine aqueous solution at 270°C and 10 MPa, which resulted in identifying the products with glycine, di-, tri-, tetra-, penta-, hexa-, hepta- and octaglycine. The peak at five minutes was the void peak of the HPLC system and the peak around six minutes mainly came from glycine anhydride including unknown products. The products of the other sample that obtained from 0.75 M diglycine were also confirmed with an HPLC profile (Data not shown). What is more, we have detected a certain amount of nonaglycine and decaglycine with the LC/MS system (Figure 2(**b**)). We have not confirmed whether undecaglycine or longer oligoglycines were produced or not. However, it is suggested that the adiabatic expansion cooling method was an effective way to obtain oligopeptides.

Figure 3 shows the concentration profiles of the products starting from glycine or diglycine. The value of concentration C_i, where i is the degree of condensation, in the two profiles wasn't considered with the compensation by the concentration when the solution was erupting and expanding to the open system. The higher the value of i, the degree of condensation of the product, was, the lower the value of C_i, the concentrations of oligoglycines, were. The profiles were so similar that we could consider that the residence time of the reaction, 27 seconds, had been sufficient to finish the two reactions, condensation and hydrolysis. It could be predicted that under hydrothermal conditions the equilibrium relations would be established between the condensation reaction and the hydrolysis reaction of oligoglycines.

Here, we calculated the rate of the loss of glycine (L) with the process as follows:

$$L = \frac{\left(C_0 - \sum iC_i^*\right)}{C_0}$$

where C_0 is defined as the concentration of material (glycine 1.0 M or diglycine 0.75 M) and C_i^* is defined as the compensated C_i by evaporation. We got the values of the loss of glycine obtained under the conditions (a) and (b) as 67 % and 68 % respectively, where the peak around six minutes in Figure 2(a) was supposed to be just composed of glycine anhydride. This indicated that more than a half of the material did not react into oligoglycine. It was possible that the material was decomposed into such compounds as ammonia, carbon dioxide and organic acids, which was inferred from Sato's study (Sato *et al.*, 2002). However we didn't analyze the side reaction.

In this paper, we demonstrated that the adiabatic expansion cooling method was one of the most proper processes of quenching the solution to polymerize peptides from amino acid. It might be thought that the adiabatic expansion cooling method made it feasible to obtain peptide easily with keeping the equilibrium stage between condensation and hydrolysis of oligopeptides at high temperature and high pressure. The hydrothermal reactor with the adiabatic expansion was so effective in polymerizing the amino acid that we could synthesize oligoglycine from glycine monomers, which could light up a new pathway not only in the field of chemical engineering but also in the study of the origin of life.

Acknowledgment

This work is partly supported by the research grant for "Learning from Nature for Production" from Sekisui Chemical Co., Ltd. and by the Ministry of Education, Culture, Sports, Science and Technology of Japan. We wish to thank Mr. S. Aizawa and Mr. S. Harada at AKICO Corporation for the design and construction of the experimental apparatus. We also thank Mr. K. Itou for the preparation of the manuscript.

Nomenclature

C_0	=	concentration of a raw material	[mM]
C_i	=	concentration of i-mer of oligoglycine	[mM]

C_i^*	=	concentation of i-mer of oligoglycine compensated by evaporation	[mM]
i	=	degree of condensation	[—]
L	=	rate of the loss of glycine	[—]

Literature Cited

Alargov, D. K., S. Deguchi, K. Tsujii and K. Horikoshi; "Reaction Behaviors of Glycine under Super- and Subcritical Water Conditions," *Origins of Life and Evolution of the Biosphere*, **32**, 1–12 (2002)

Imai, E., H. Honda, K. Hatori, A. Brack and K. Matsuno; "Elongation of Oligopeptides in a Simulated Submarine Hydrothermal System," *Science*, **283**, 831–833 (1999)

Islam, M. N., T. Kaneko and K. Kobayashi; "Reaction of Amino Acids in a Supercritical Water-Flow Reactor Simulating Submarine Hydrothermal Systems," *Bull. Chem. Soc. Jpn.*, **76**, 1171–1178 (2003)

Ogata, Y., E. Imai, H. Honda, K. Hatori and K. Matsuno; "Hydrothermal Circulation of Seawater through Hot Vents and Contribution of Interface Chemistry to Prebiotic Synthesis," *Origins of Life and Evolution of the Biosphere*, **30**, 527–537 (2000)

Pearson, J. D. and M. C. McCroskey; "Perfluorinated Acid Alternatives to Trifluoroacetic Acid for Reversed-Phase High-Performance Liquid Chromatography," *J. Chromatogr., A*, **746**, 277–281 (1996)

Sato, N., H. Daimon and K. Fujie; "Decomposition of Glycine in High Temperature and High Pressure Water," *Kagaku Kogaku Ronbunshu*, **28**, 113–117 (2002)

Shock, E. L.; "Stability of Peptides in High-Temperature Aqueous Solutions," *Geochimi. Cosmochim. Acta*, **56**, 3481–3491 (1992)

Tucker, I. G., M. E. Dowty, M. Veillard, M. A. Longer and J. R. Robinson; "Reversed-Phase High-Performance Liquid Chromatographic Analysis of Oligoglycines (One to Six Amino Acid Residues)," *Pharm. Res.*, **6**, 100–102 (1989)

Novel Surface Processing with Sulfonic Acid for Quantum Dot and Its Characteristics

Amane SHIOHARA, Noriyoshi MANABE,
Kazumi OMATA and Kenji YAMAMOTO
Department of Medical Ecology and Informatics,
Research Institute, International Medical Center of Japan,
21-1, Toyama 1, Shinjyuku-ku, Tokyo 162-8655, Japan

Keywords: QD-SO_3^-, Surface Processing, Sulfonic Acid, Acidic Conditions

We developed smaller sized quantum dots covered with sodium 2-mercaptoethanesulfonate which has a sulfonyl group (QDs-SO_3^-), and compared its stability in acid, salt and buffer solutions with that of the quantum dots covered with the mercaptoundecanoic acid (QDs-MUA) and covered with the NH_2 group (QDs-NH_2). We found that the QD-SO_3^- well disperses in these solutions without quenching and this stability holds on for 24 h. Next, we investigated the effect of Sheep Serum Albumin (SSA) coating. The SSA coating stabilizes the QD-MUA in the solutions. However, for the QD-SO_3^-, it does not have any significant effect. It implies that the QD-SO_3^- has advantages over the other quantum dots on the stability in the solutions. These results suggest that the novel surface processing using the sulfonyl group expands the possibilities of applications for various fields.

Introduction

The nanometer-size semiconductor is called a quantum dot (QD). The quantum dots are characterized by the following quantum effects: (1) a special photo quality caused by widening the band gap when the spatial dimension is reduced (Unold *et al.*, 2004; Weig *et al.*, 2004); (2) they can produce different colors by changing the sizes (Mattoussi *et al.*, 2000); and (3) they have excellent photostability and their fluorescences can be observed more than 1 h (Hoshino *et al.*, 2004). Because of these interesting characteristics, quantum dots are widely employed for industrial and medical applications. For the industrial applications, they are used as photovoltaics, multicolor LEDs, electronic memory devices, quantum dot barcodes, high throughput chemical and biological sensors (Han *et al.*, 2001; Coe *et al.*, 2002; Santori *et al.*, 2002; Zrenner *et al.*, 2002; Alivisatos., 2004; Clapp *et al.*, 2004). For the medical applications, they are coming into use as immunostaining, a drug delivery system, and so on (Dubertret *et al.*, 2002; Xu *et al.*, 2003; Shiohara *et al.*, 2004). Here, one of the indispensable properties for both applications is their interactions with other materials; especially the interaction with water plays a crucial role for the dispersibility in aqueous solutions. For example, this property is important for integrating quantum dots into devices functionally (Jaffer *et al.*, 2004). A simple way to control the solvation is to modify the surface of the quantum dots. The surface-modified quantum dots synthesized for the first time are covered with non-polar groups of organic molecules such as trioctyl phosphine oxide (TOPO), so that they are insoluble in water, putting some limitations on their functions in aqueous conditions. This problem was solved by Chan and Nie (1998). They synthesized water-soluble quantum dots, CdSe/QD-MUA, the surface of which are covered with mercaptoundecanoic acid (MUA). This QD-MUA was made by the method of substituting non-polar groups of organic molecules on the surface of quantum dots for MUA. The QD-MUA made a tremendous contribution to the possibility of application of quantum dots for various fields not only industry but also medical biology (Huang *et al.*, 1998; Åkerman *et al.*, 2002; Hanaki *et al.*, 2003; Gao *et al.*, 2004; Hoshino *et al.*, 2004; Wu and Bruchez, 2004; Santra *et al.*, 2005).

A further important problem is that the QD-MUA is not stable in acid or it coheres easily in buffer solution. This should be an impediment to medical 3 applications, and it might also cause a problem in the field of industry. Hanaki *et al.* (2003) have succeeded to stabilize QD-MUA under physiological conditions by coating it with sheep serum albumin (SSA), and the purpose of the present work is to develop their study. We investigated CdSe/QD covered with sodium 2-mercaptoethanesulfonate (QD-SO_3^-) and focused on its compatibility with various solvents. The reasons we chose this ligand are as follows. First, the sulfonyl group is a strong acid, and secondly this ligand can be

Received on May 18, 2005. Correspondence concerning this article should be addressed to K. Yamamoto (E-mail address: backen@ri.imcj.go.jp).

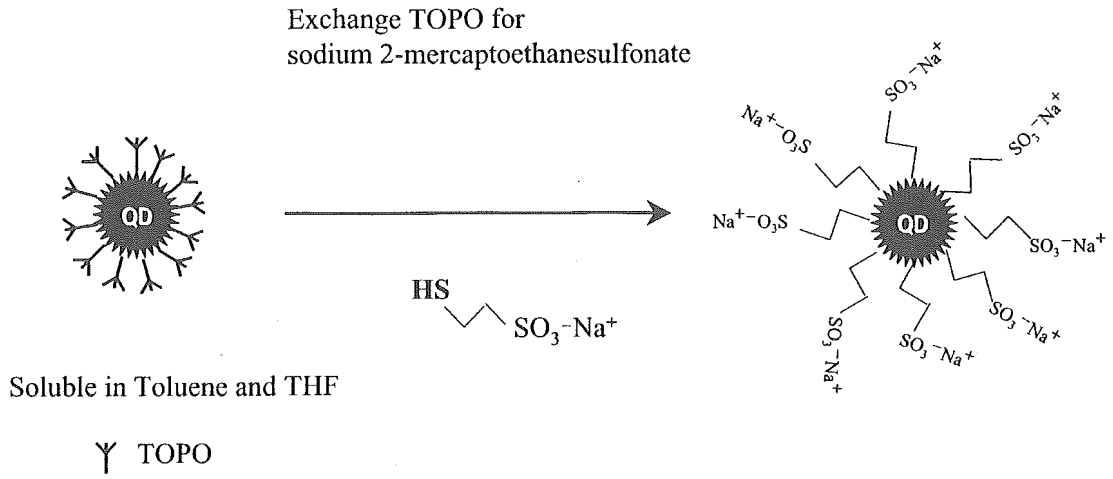

Fig. 1 Synthesis of QD-SO_3^-

connected with an alkyl chain followed by the terminal group, SH. In this study, (1) we succeeded in synthesis of QD-SO_3^- for the first time; (2) we compared the stability of QD-SO_3^- with that of quantum dots with NH_2 connected to two alkyl groups (QD-NH_2) and QD-MUA in acid and buffer solutions; and (3) we studied those quantum dots coated with SSA to conduct the experiments under conditions similar to Hanaki *et al.* (2003).

1. Materials and Methods

1.1 Preparation of QD-MUA, QD-NH_2 and QD-SO_3^-

The quantum dots with the core of CdSe and the shell of ZnS (see **Figure 1**) were synthesized from the QD-tri-*n*-octylphosphine oxide (QD-TOPO). After QD-TOPO (Murray *et al.*, 1993; Hines and Guyot-Sionnest, 1996; Peng *et al.*, 1997) dissolved in tetrahydrofuran (Wako Pure Chemical Industries, Ltd.), the solution was warmed up to 85°C, and sodium 2-mercaptoethanesulfonate (Shionogi & Co., Ltd.), MUA (Sigma-Aldrich Co.) and cysteamine hydrochloride (Wako Pure Chemical Industries, Ltd.) dissolved in ethanol were dripped into it. It was reflexed for 12 h. Then, for the sodium 2-mercaptoethanesulfonate and MUA, 100 μL of the NaOH solution (pH 10) was added into them to ionize the quantum dots, and the tetrahydrofuran was evaporated at 90°C. The unrefined quantum dots thus obtained, were refined and concentrated with an ultrafiltration membrane (Microcon YM-3, Millipore Corp.) and sephadex column (MicroSpin G-25 Columns, Amersham Bioscience Corp.), and then each of the refined quantum dot was obtained. To coat the quantum dots with SSA, we mixed the solutions of quantum dots and SSA.

1.2 Preparation of acid, buffer and salt solutions

The acidic conditions were provided by sulfuric acid. The observation range was 0.25 mM (pH 3.2)–0.001 mM (pH 5.1). The pH of borate buffer solution was pH 9. The concentration of the salt solutions were 1 M NaCl and 5 M NaCl. The PBS and MEM were used as salt solutions as well. The concentration of QD-MUA, QD-NH_2, and QD-SO_3^- was 0.1 mg/mL. As for these quantum dots, the powder of each quantum dot was weighed and 10 mg/mL aqueous solution was made. Then the solutions were diluted into 0.1 mg/mL. The quantum dots were added to each solution and they were observed 1 h and 24 h after.

Table 1 Particle size and surface potential of each quantum dot

	Particle size [nm]	Zeta potential [mV]
QD-SO_3	10.12	−32.74
QD-MUA	19.97	−32.31
QD-NH_2	10.36	10.95

The particle size and surface potential of each quantum dot was measured with Zetasizer (Malvern Instruments Ltd.) after filtration. A 0.45 μm filter was used for this experiment.

2. Result

2.1 Spectrum intensity, size distribution, and zeta potential

We measured the fluorescent intensity of QD-MUA, QD-NH_2, and QD-SO_3^-. The spectra are shown in **Figure 2**. The fluorescent peak intensity of QD-MUA was about 3 times as large as that of QD-SO_3^-. However, that of QD-NH_2 was 3 times lower than that of QD-SO_3^-.

The results of the particle sizes and the zeta potential are shown in **Table 1**. The particle diameter of QD-SO_3^- is 10.12 ± 3.247 nm. On the other hand, 80% of the provided QD-MUA have the particle diameter